NUMERICAL ANALYSIS OF CONTACT FORCES AT THE TOUCHDOWN ZONE (TDZ) OF FLEXIBLE RISERS

Carlos Eduardo da Silva

Leandro Carlos Gazoni

Marcus Vinícius Casagrande

José Luis Drummond Alves

kadu@lamce.coppe.ufrj.br

lgazoni@gmail.com

marcusscasagrande@gmail.com

jalves@lamce.coppe.ufrj.br

Civil Engineering Program, COPPE/UFRJ

Av. Athos da Silveira Ramos, 149 – Ilha do Fundão, CEP: 21941-909 Rio de Janeiro - RJ

Mario Alfredo Vignoles

mavignoles@technip.com

TechnipFMC

Rua Dom Marcos Barbosa, 02 - 4° andar, CEP 20211-178, Rio de Janeiro - RJ

Abstract. *In the oil and gas industry, current technology for flexible risers and flowlines technology for deep and ultra-deep-water operation requires more realistic simulation tools and calculation methods every day. This work addresses a topic that represent, among others, one of the critical bottlenecks currently faced for the application of the flexible riser solution in the pre-salt projects in ultra-deep waters, i.e., the analysis of cross section forces at the touchdown zone (TDZ) and touch down point (TDP). Dynamic simulations performed in state-of-the-art program, usually present good agreement and reliable results for sections away from the strongly dynamic riser and soil interaction region (TDP-TDZ region). Some simulations in the TDP region, present very high compression and very low bending radii and may, in some cases, render the flexible solution unfeasible. There is also a large difference in results between programs in this region. At present, global analyzes are performed considering the rigid soil, thus ensuring conservatism in the results, since there are no experimental models or results of real-scale measurements for flexible tubes to guarantee* *more realistic or less conservative results.This work presents a specially tailored model for the global and local dynamic simulation of riser soil interaction. The model accounts the nonlinear soil behavior modeled with 3D solid elements and contact impact interaction at TDZ with the riser structure, modeled with 3D beam elements. Soil behavior were calibrated with a set of tests in a centrifuge apparatus while riser dynamics was calibrated with reduced model tests carried out on an ocean tank at COPPE/UFRJ.*

A series of benchmark tests were performed for usual riser configurations. Results of the proposed approach are assessed in the light of state-of-the art codes with respect to curvature and compression at cross sections along the riser, deformation and stresses in the underlying soil mass.

Keywords: *Numerical Modeling, Touchdown point (TDP), Flexible Riser*

1 INTRODUCTION

In recent years, the use of flexible risers has increased significantly in deep and ultra-deep water oil and gas production. In such large depths, catenary risers are an important solution due to their lower installation cost. Usually, the motion of the floating vessel imposes an excitation at the top of the riser, which is one of the main causes of the general dynamic response of the riser. Therefore, the dynamic analysis of the riser is a key issue on offshore floating units that requires a proper formulation of the theoretical model to correctly represent the response (Chatjigeorgiou, 2008).

One of the critical issues in the design of flexible risers to estimate its fatigue life near its touchdown zone (TDZ), which is constrained by seabed soil. Fatigue is a progressive and localized structural damage that occurs when an object is subjected to cyclic loadings. Fatigue in riser results mainly from the variation of the bending moment along the riser due to its oscillatory motion. According to Bhat et al. (2004), the most probable hotspots of fatigue damage are near upper end where the riser is attached to the floating structure and the TDZ where it contacts the seabed.

The proposed methodology of this work is based on the finite elements method (FEM). A bidimensional beam element with large displacement formulation is presented. For the integration in the time domain, the Newmark method is used (O'Brien et al., 1989).

2 MATHEMATICAL FORMULATION

The 2D nonlinear dynamic problem of a beam is considered. Due to large displacements of the riser, a geometric nonlinear element is utilized.

2.1 The Newmark method

According to Hughes (2012), the most widely used family of direct methods for solving the equation of motion (Eqs. (1), (2) and (3)) is the Newmark family. It consists of a method of numerical integration in the time domain.

$$\boldsymbol{M}\ddot{\boldsymbol{u}} + \boldsymbol{C}\dot{\boldsymbol{u}} + \boldsymbol{K}\boldsymbol{u} = \boldsymbol{F} \tag{1}$$

$$\boldsymbol{u}(0) = \boldsymbol{u_0} \tag{2}$$

$$\dot{\boldsymbol{u}}(0) = \boldsymbol{v_0} \tag{3}$$

where $\boldsymbol{M}$ is the mass matrix, $\boldsymbol{C}$ is the viscous damping matrix, $\boldsymbol{K}$ is the stiffness matrix, $\boldsymbol{F}$ is the vector of applied forces, $\boldsymbol{u}$ is the displacement vector, $\dot{\boldsymbol{u}}$ is the velocity vector and $\ddot{\boldsymbol{u}}$ is the acceleration vector. The matrices $\boldsymbol{M}$, $\boldsymbol{C}$ and $\boldsymbol{K}$ are supposed to be symmetric; $\boldsymbol{M}$ is positive-definite, and $\boldsymbol{C}$ and $\boldsymbol{K}$ are positive semi-definite.

Using finite difference formulation to describe the evolution of the approximate solution, the equations of Newmark family are presented in Eqs. (4), (5) and (6).

$$\boldsymbol{M}\boldsymbol{a}_{t+\Delta t} + \boldsymbol{C}\boldsymbol{v}_{t+\Delta t} + \boldsymbol{K}\boldsymbol{u}_{t+\Delta t} = \boldsymbol{F}_{t+\Delta t} \tag{4}$$

$$\boldsymbol{u}_{t+\Delta t} = \boldsymbol{u}_t + \Delta t\ \boldsymbol{v}_t + \frac{\Delta t^2}{2}[(1-2\beta)\boldsymbol{a}_t + 2\beta\ \boldsymbol{a}_{t+\Delta t}] \tag{5}$$

$$\boldsymbol{v}_{t+\Delta t} = \boldsymbol{v}_t + \Delta t\ [(1-\gamma)\boldsymbol{a}_t + \gamma\ \boldsymbol{a}_{t+\Delta t}] \tag{6}$$

where $\boldsymbol{u}_t$, $\boldsymbol{v}_t$ and $\boldsymbol{a}_t$ are the approximations of the displacement, velocity and acceleration vectors at time *t*, respectively. The parameters γ and β determine the stability and accuracy characteristics of the algorithm.

Usually, Eqs. (5) and (6) are inserted in Eq. (4) to calculate the only unknown $\boldsymbol{a}_{t+\Delta t}$ and subsequently $\boldsymbol{u}_{t+\Delta t}$ and $\boldsymbol{v}_{t+\Delta t}$ are calculated. This implementation is called the *a-form*.

However, non-linear problems are normally solved in the *u-form*. Equations (5) and (6) can be rewritten isolating the terms relative to the velocity and acceleration, resulting in:

$$\boldsymbol{v}_{t+\Delta t} = \frac{\gamma}{\beta\ \Delta t}(\boldsymbol{u}_{t+\Delta t} - \boldsymbol{u}_t) - \left(\frac{\gamma}{\beta} - 1\right)\ \boldsymbol{v}_t - \left(\frac{\gamma}{2\beta} - 1\right)\Delta t\ \boldsymbol{a}_t \tag{7}$$

$$\boldsymbol{a}_{t+\Delta t} = \frac{1}{\beta\ \Delta t^2}(\boldsymbol{u}_{t+\Delta t} - \boldsymbol{u}_t) - \frac{1}{\beta\ \Delta t}\ \boldsymbol{v}_t - \left(\frac{1}{2\beta} - 1\right)\boldsymbol{a}_t \tag{8}$$

Once the velocity and acceleration are written as a function of the displacement, the equation of motion can be solved for the displacement at time *t+Δt*, and subsequently the velocity and acceleration.

The basic problem in a general nonlinear dynamic analysis is to find the solution of the equation of motion according to the applied loads:

$$\boldsymbol{M}\boldsymbol{a}_{t+\Delta t} = \boldsymbol{R}_{t+\Delta t} - \boldsymbol{F}_{t+\Delta t} \tag{9}$$

where $\boldsymbol{R}_{t+\Delta t}$ is the vector of externally applied nodal forces at time *t* and $\boldsymbol{F}_{t+\Delta t}$ is the vector of internal forces in the configuration of time *t*. For an iterative solution (Bathe, 2006), Eq. (9) has the form:

$$\boldsymbol{M}\boldsymbol{a}_{t+\Delta t}^{(\boldsymbol{k})} = \boldsymbol{R}_{t+\Delta t} - \boldsymbol{F}_{t+\Delta t}^{(\boldsymbol{k})} \tag{10}$$

The superscript indicates that the equation is being evaluated at iteration *k*. In this equation, the vector of external forces does not have the superscript since it does not depend on the iteration. For consistency, a null superscript indicates that the variable should be evaluated at the previous time step, i.e., at time *t*.

The vector of internal forces is a nonlinear function of the displacement. To linearize this vector, the previous internal force evaluated is used, and the vector is linearized at that point.

$$\boldsymbol{F}_{t+\Delta t}^{(\boldsymbol{k})} = \boldsymbol{F}_{t+\Delta t}^{(\boldsymbol{k-1})} + \boldsymbol{\Delta F}^{(\boldsymbol{k})} \tag{11}$$

$$\boldsymbol{\Delta F}^{(\boldsymbol{k})} = \boldsymbol{K}_{t+\Delta t}^{(\boldsymbol{k-1})}\boldsymbol{\Delta u}^{(\boldsymbol{k})} \tag{12}$$

$$\boldsymbol{K}_{t+\Delta t}^{(\boldsymbol{k-1})} = \frac{\partial \boldsymbol{F}_{t+\Delta t}^{(k-1)}}{\partial \boldsymbol{u}_{t+\Delta t}^{(k-1)}} \tag{13}$$

where $\boldsymbol{K}_{t+\Delta t}^{(k-1)}$ is the tangent stiffness matrix which corresponds to the derivative of the internal force $\boldsymbol{F}_{t+\Delta t}^{(k-1)}$ with respect to the nodal point displacement $\boldsymbol{u}_{t+\Delta t}^{(k-1)}$ at the previous available result. Then, Eq. (10) can be rewritten as:

$$\boldsymbol{M}\boldsymbol{a}_{t+\Delta t}^{(k)} = \boldsymbol{R}_{t+\Delta t} - \boldsymbol{F}_{t+\Delta t}^{(k-1)} - \boldsymbol{K}_{t+\Delta t}^{(k-1)}\boldsymbol{\Delta u}^{(k)} \tag{14}$$

Including a viscous force and rearranging the terms, Eq. (14) turns into:

$$\boldsymbol{M}\boldsymbol{a}_{t+\Delta t}^{(k)} + \boldsymbol{C}\boldsymbol{v}_{t+\Delta t}^{(k)} + \boldsymbol{K}_{t+\Delta t}^{(k-1)}\boldsymbol{\Delta u}^{(k)} = \boldsymbol{R}_{t+\Delta t} - \boldsymbol{F}_{t+\Delta t}^{(k-1)} \tag{15}$$

Using the Newton-Raphson method to find the solution of Eq. (15), the displacement at the current iteration *(k)*, $\boldsymbol{u}_{t+\Delta t}^{(k)}$ is decomposed into the displacement at the previous iteration *(k-1)*, $\boldsymbol{u}_{t+\Delta t}^{(k-1)}$, and a variation of the displacement, $\boldsymbol{\Delta u}^{(k)}$:

$$\boldsymbol{u}_{t+\Delta t}^{(k)} = \boldsymbol{u}_{t+\Delta t}^{(k-1)} + \boldsymbol{\Delta u}^{(k)} \tag{16}$$

Implementing the Newton-Raphson method in the Newmark family equations, the following equations are obtained:

$$\boldsymbol{v}_{t+\Delta t}^{(k)} = \frac{\gamma}{\beta\,\Delta t}\left(\boldsymbol{u}_{t+\Delta t}^{(k-1)} + \boldsymbol{\Delta u}^{(k)} - \boldsymbol{u}_t\right) - \left(\frac{\gamma}{\beta} - 1\right)\,\boldsymbol{v}_t - \left(\frac{\gamma}{2\beta} - 1\right)\Delta t\;\boldsymbol{a}_t \tag{17}$$

$$\boldsymbol{a}_{t+\Delta t}^{(k)} = \frac{1}{\beta\,\Delta t^2}\left(\boldsymbol{u}_{t+\Delta t}^{(k-1)} + \boldsymbol{\Delta u}^{(k)} - \boldsymbol{u}_t\right) - \frac{1}{\beta\,\Delta t}\,\boldsymbol{v}_t - \left(\frac{1}{2\beta} - 1\right)\boldsymbol{a}_t \tag{18}$$

Substituting Eqs. (17) and (18) in Eq. (15), and selecting the variation of the displacement as the main unknown, the final equation can be written in a reduced form as:

$$\widehat{\boldsymbol{K}}_{t+\Delta t}^{(k-1)}\boldsymbol{\Delta u}^{(k)} = \boldsymbol{R}_{t+\Delta t} - \widehat{\boldsymbol{F}}_{t+\Delta t}^{(k-1)} \tag{19}$$

where $\widehat{\boldsymbol{K}}_{t+\Delta t}^{(k-1)}$ is the effective tangent stiffness matrix and $\widehat{\boldsymbol{F}}_{t+\Delta t}^{(k-1)}$ is the effective internal force vector.

$$\widehat{\boldsymbol{K}}_{t+\Delta t}^{(k-1)} = \left[\frac{1}{\beta\,\Delta t^2}\boldsymbol{M} + \frac{\gamma}{\beta\,\Delta t}\boldsymbol{C} + \boldsymbol{K}_{t+\Delta t}^{(k-1)}\right] \tag{20}$$

$$\widehat{\boldsymbol{F}}_{t+\Delta t}^{(k-1)} = \boldsymbol{F}_{t+\Delta t}^{(k-1)} + \boldsymbol{M}\widetilde{\boldsymbol{a}}_{t+\Delta t}^{(k-1)} + \boldsymbol{C}\widetilde{\boldsymbol{v}}_{t+\Delta t}^{(k-1)} \tag{21}$$

The terms $\widetilde{\boldsymbol{v}}_{t+\Delta t}^{(k-1)}$ and $\widetilde{\boldsymbol{a}}_{t+\Delta t}^{(k-1)}$ are respectively called the predicted velocity and acceleration vectors.

$$\widetilde{\boldsymbol{v}}_{t+\Delta t}^{(k-1)} = \frac{\gamma}{\beta\,\Delta t}\left(\boldsymbol{u}_{t+\Delta t}^{(k-1)} - \boldsymbol{u}_t\right) - \left(\frac{\gamma}{\beta} - 1\right)\,\boldsymbol{v}_t - \left(\frac{\gamma}{2\beta} - 1\right)\Delta t\;\boldsymbol{a}_t \tag{22}$$

$$\widetilde{\boldsymbol{a}}_{t+\Delta t}^{(k-1)} = \frac{1}{\beta\,\Delta t^2}\left(\boldsymbol{u}_{t+\Delta t}^{(k-1)} - \boldsymbol{u}_t\right) - \frac{1}{\beta\,\Delta t}\,\boldsymbol{v}_t - \left(\frac{1}{2\beta} - 1\right)\boldsymbol{a}_t \tag{23}$$

The solution of the system can be found inverting the effective tangent stiffness matrix and solving Eq. (19) for the variation of the displacement. To complete the time cycle the displacement, velocity and acceleration are updated via Eqs. (9), (24) and (25).

$$\boldsymbol{v}_{t+\Delta t}^{(k)} = \widetilde{\boldsymbol{v}}_{t+\Delta t}^{(k-1)} + \frac{\gamma}{\beta\,\Delta t}\boldsymbol{\Delta u}^{(k)} \tag{24}$$

$$\boldsymbol{a}_{t+\Delta t}^{(k)} = \tilde{\boldsymbol{a}}_{t+\Delta t}^{(k-1)} + \frac{1}{\beta\,\Delta t^2}\boldsymbol{\Delta u}^{(k)} \tag{25}$$

2.2 Total Lagrangian method

The total Lagrangian method is appropriate for large rotations and small strains, which is the case of the risers. When large deflections are present, the equations of force equilibrium must be formulated for the deformed configuration of the element. To account for the effects of changes in the geometry, as the external force is applied, the solution of the nonlinear problem is linearized in a sequence of steps, each one representing a load step or a time step. However, due to the presence of large deflections, strain-displacement equations contain nonlinear terms, which must be included when calculating the stiffness matrix (Przemieniecki, 1985).

The nonlinear terms in the strain-displacement equation modify the element stiffness matrix $\boldsymbol{K^e}$ so that

$$\boldsymbol{K^e} = \boldsymbol{K_E^e} + \boldsymbol{K_G^e} \tag{26}$$

where $\boldsymbol{K_E^e}$ is the linear elastic stiffness matrix and $\boldsymbol{K_G^e}$ is the geometrical stiffness matrix, both of which are calculated for the element at the start of each iteration.

$$\boldsymbol{K_E^e} = \frac{EI}{L^3}\begin{bmatrix} \frac{AL^2}{I} & & & & Sym. & \\ 0 & 12 & & & & \\ 0 & 6L & 4L^2 & & & \\ -\frac{AL^2}{I} & 0 & 0 & \frac{AL^2}{I} & & \\ 0 & -12L & -6L & 0 & 12 & \\ 0 & 6L & 2L^2 & 0 & -6L & 4L^2 \end{bmatrix} \tag{27}$$

$$\boldsymbol{K_G^e} = \frac{N}{L}\begin{bmatrix} 0 & & & & Sym. & \\ 0 & \frac{6}{5} & & & & \\ 0 & \frac{L}{10} & \frac{2}{15}L^2 & & & \\ 0 & 0 & 0 & 0 & & \\ 0 & -\frac{6}{5} & -\frac{L}{10} & 0 & \frac{6}{5} & \\ 0 & \frac{L}{10} & -\frac{L^2}{30} & 0 & -\frac{L}{10} & \frac{2}{15}L^2 \end{bmatrix} \tag{28}$$

where L is the element length, I the area moment of inertia, E the modulus of elasticity, and N the element internal axial force.

The rigid body motion in finite elements can create residual stress due to do the large displacements of the element. To outline this issue, a natural displacement vector $\boldsymbol{u_n^e}$ is defined (Paraski, 2012; Souza, 2000; Kordkheili et al., 2011). This natural displacement in the total lagrangian method represents the stress-related displacements in a local referential. For each element, the global displacement vector is defined as:

Proceedings of the XXXVIII Iberian Latin-American Congress on Computational Methods in Engineering
P.O. Faria, R.H. Lopez, L.F.F. Miguel, W.J.S. Gomes, M. Noronha (Editores), ABMEC, Florianópolis, SC, Brazil, November 5-8, 2017.

$$\boldsymbol{u^e} = \begin{Bmatrix} u_1 \\ v_1 \\ \theta_1 \\ u_2 \\ v_2 \\ \theta_2 \end{Bmatrix} \tag{29}$$

where u_i is the displacement in horizontal direction of node i, v_i is the displacement in vertical direction of node i, and θ_i is the angular displacement of node i. The local referential is defined with the origin at node 1, so there is no horizontal or vertical displacement at this node, and the first principal direction passes through node 2, which causes no vertical displacement at node 2. For each element, the natural displacement vector is defined as:

$$\boldsymbol{u_n^e} = \begin{Bmatrix} 0 \\ 0 \\ \varphi_1 \\ \delta \\ 0 \\ \varphi_2 \end{Bmatrix} \tag{30}$$

where,

$$\delta = L_{t+\Delta t} - L_{t=0} \tag{31}$$

$$\varphi_1 = \theta_1 - \Psi \tag{32}$$

$$\varphi_2 = \theta_2 - \Psi \tag{33}$$

$$v = v_2 - v_1 \tag{34}$$

$$u = u_2 - u_1 \tag{35}$$

$$\Psi = tan^{-1}\left(\frac{v}{L_{t+\Delta t} + u}\right) \tag{36}$$

However, the stiffness matrix of the element is defined in the local referential. To transform the local referential to global, a rotation matrix is defined:

$$\boldsymbol{R^e} = \begin{bmatrix} cos\,(\Psi) & sin\,(\Psi) & 0 & 0 & 0 & 0 \\ -sin\,(\Psi) & cos\,(\Psi) & 0 & 0 & 0 & 0 \\ 0 & 0 & 1 & 0 & 0 & 0 \\ 0 & 0 & 0 & cos\,(\Psi) & sin\,(\Psi) & 0 \\ 0 & 0 & 0 & -sin\,(\Psi) & cos\,(\Psi) & 0 \\ 0 & 0 & 0 & 0 & 0 & 1 \end{bmatrix} \tag{37}$$

The element internal force vector $\boldsymbol{F^e}$ can be evaluated through the natural displacement vector $\boldsymbol{u_n^e}$ and the linear stiffness matrix $\boldsymbol{K_E^e}$.

$$\boldsymbol{F^e} = [\boldsymbol{R^e}^{\boldsymbol{T}}\boldsymbol{K_E^e}\,\boldsymbol{R^e}]\boldsymbol{u_n^e} \tag{38}$$

The internal force vector $\boldsymbol{F_{t+\Delta t}^{(k-1)}}$ is the assembly of all element internal force vectors. Analogously, the tangent stiffness matrix $\boldsymbol{K_{t+\Delta t}^{(k-1)}}$ is the assembly of all element stiffness matrix rotated to the global coordinate of system $[\boldsymbol{R^e}^{\boldsymbol{T}}\boldsymbol{K^e}\boldsymbol{R^e}]$.

Proceedings of the XXXVIII Iberian Latin-American Congress on Computational Methods in Engineering
P.O. Faria, R.H. Lopez, L.F.F. Miguel, W.J.S. Gomes, M. Noronha (Editores), ABMEC, Florianópolis, SC, Brazil, November 5-8, 2017.

Finally, the element mass matrix $\boldsymbol{M^e}$, in its local referential, is defined as:

$$\boldsymbol{M^e} = \frac{\rho AL}{420}\begin{bmatrix} 140 & & & & & \\ 0 & 156 & & & Sym. & \\ 0 & 22L & 4L^2 & & & \\ 70 & 0 & 0 & 140 & & \\ 0 & 54 & 13L & 0 & 156 & \\ 0 & -13L & -3L^2 & 0 & -22L & 4L^2 \end{bmatrix} \tag{39}$$

2.3 Penalty method

The penalty method introduces a force component at the nodes of the beam elements that have penetrated the soil surface with the purpose of eliminating the penetration. The computed force is proportional to the penetration when it is present (Eq. 40), and is null when there is no penetration.

$$\boldsymbol{F_c} = \boldsymbol{k_c} \cdot \boldsymbol{\delta_c} \tag{40}$$

where $\boldsymbol{F_c}$ is the contact force, $\boldsymbol{k_c}$ is represents the penalty stiffness and $\boldsymbol{\delta_c}$ is the actual penetration of the node in the target surface.

Despite this method being simple and largely used, a consistent structure must be created in the algorithm of the code. To the specific case of the riser-soil interaction, the surrounding surface of the soil is initially mapped into a target surface mesh, then, in every iteration of each time step, it is verified if there is penetration between each node of the beam elements and the target surface of the soil. If a penetration is present, the penalty force is computed and distributed to the node of the beam and to the nodes of the soil element.

3 RESULTS

3.1 Flexible riser in a catenary mode

In this case, a flexible riser in a catenary mode is analyzed. The system consists of a flexible riser with length of 350.0m, the upper point is connected to a surface floater displaced 150.0 m horizontally and 150.0 m vertically from the lowest point, fixed to a sub-sea tower (Figure 1). Both ends can freely rotate. The riser was divided into 35 elements with 10 meters of length each. It is assumed that the riser is filled with seawater. A similar system was studied by Yazdchi & Crisfield (2002), from which the results are compared.

The mass density of seawater is taken as 1025.0 kg/m³ and the mass per unit length of the riser is considered to be 57.5 kg/m. The riser geometry is defined by an external diameter of 0.26 m and an internal diameter of 0.20 m. The bending stiffness of the riser is 20.96e3 N.m² and the axial stiffness is 15.38e8 N/m. Additionally, hydrodynamic effects are included considering the Morison equation. The transverse drag coefficient is 1.0 and the tangential drag coefficient is 0.0.

The dynamic analysis has been implemented in three stages. First, the riser geometry is horizontal with the left lower point fixed, then the riser is allowed to sag under self-weight and buoyancy forces. In the second stage, the right point is moved to the surface floater. These procedures are necessary to develop the correct stress distribution over the riser in catenary mode.

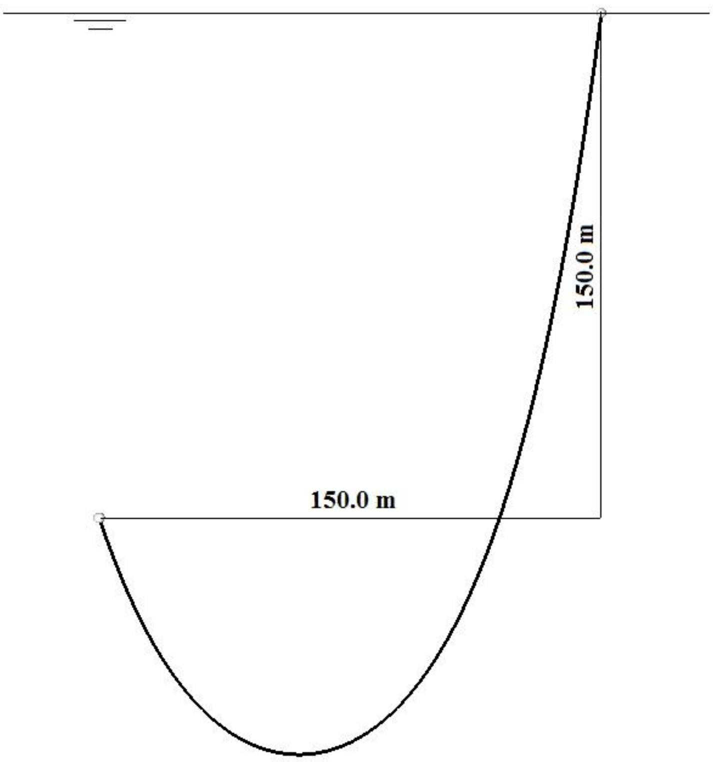

Fig. 1: Flexible riser catenary configuration.

The third stage is a surge motion of the surface floater. This motion represents the displacement due to ship movement. The surge motion consists in an excitation of amplitude 2.01 m and a corresponding period of 14.0 s.

The results of the first two stages are presented in Table 1 and Figure 2. Table 1 presents the vertical reaction (V), the horizontal reaction (H) and the angle of the riser (θ) of the lower point (subscribe 1) and of the upper point (subscribe 2). Figure 2 shows the bending moment diagram of the flexible riser in its final configuration. The comparison between the works shows excellent agreement.

Table 1: Nodal reactions and angle of the riser

	V_1(kN)	**V_2**(kN)	**H_1**(kN)	**H_2**(kN)	**θ_1**(deg)	**θ_2(deg)**
Yazdchi & Crisfield (2002)	35.86	91.61	12.04	12.04	71.17	82.46
Present work	35.79	91.4	11.76	11.9	70.94	82.44

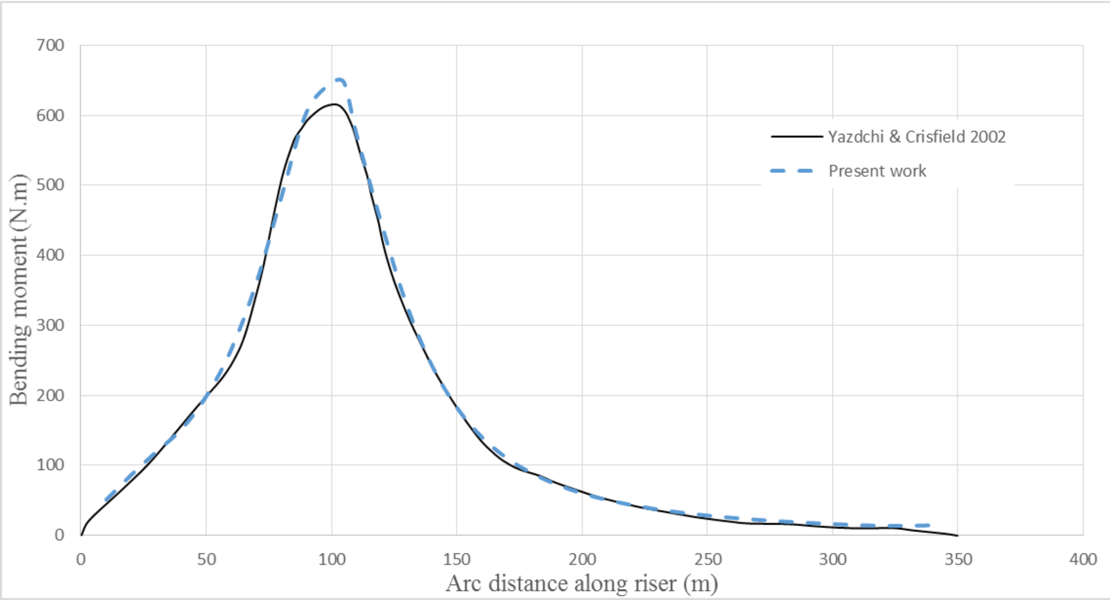

Fig. 2: Bending moment distribution along the riser.

The third stage excites the riser dynamically. The results of this analysis are shown in Figure 3. Considering the floater's movement imposes moderately large displacement to the flexible riser, there is a good agreement between the implementation of this work and Yazdchi & Crisfield (2002).

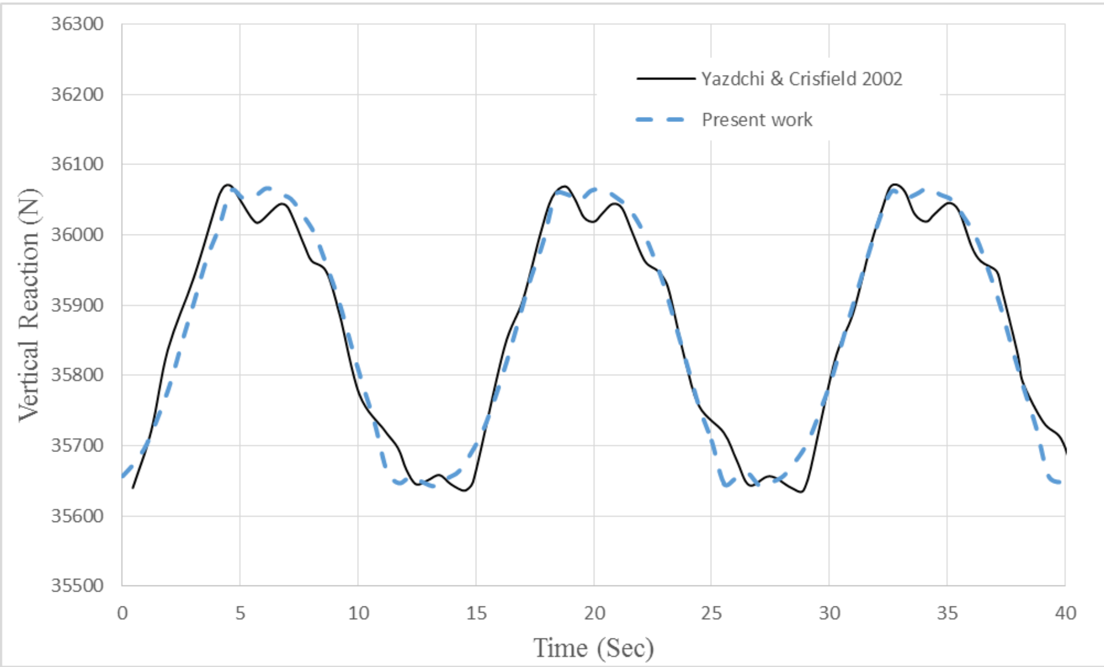

Fig. 3: Dynamic response of the riser.

3.2 Flexible riser in contact with the soil

This section presents a comparative assessment of a flexible riser in contact with the soil. The numerical results from TDPPLEX software, implemented with the formulation presented above, is compared with DEEPLINES software. The results involve time-history of some variables, such as: Axial force at the top and bottom connections, displacement at the hanging and TDZ region.

The set-up of the simulation is presented at Figure 4. A flexible riser, with 0.15m diameter and 40m length inside a 15 meters depth water tank (Cm = 2.0, Cd = 1.2), is excited by an oscillator with an amplitude of 20 degrees, a radius of gyration of 2 meters and a period of 10 seconds. The riser has 1.MN axial stiffness, 1kN.m² bending stiffness and a weight of 15.00 kgf/m. The forces on the riser near the TPZ were assessed considering a riser seated directly on the rigid floor of tank.

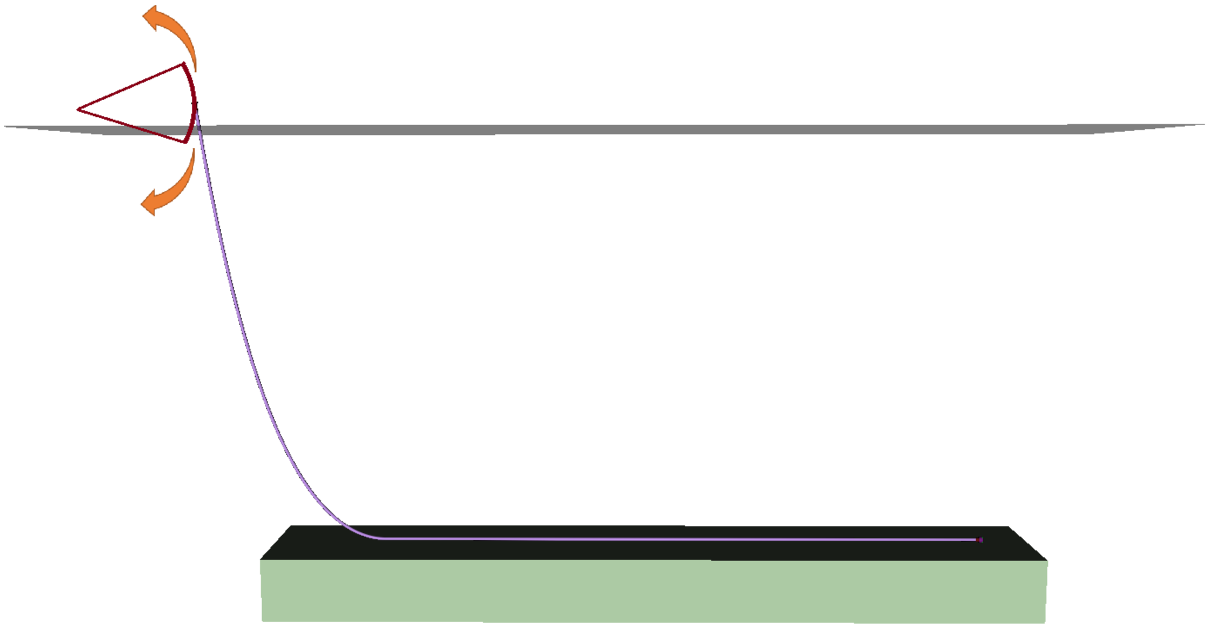

Fig. 4: Schematic of the top oscillator (red).

Regarding attention to axial force results at top (Figure 5), is possible to mention that both results from TDPFLEX and DEEPLINES are in good agreement for period and amplitude. For the axial force at bottom, the Figure 5 shows that the axial force of TDPFLEX and DEEPLINES are very similar too.

Illustrating the displacement results, Figure 6 shows an excellent agreement between the vertical and horizontal positions of the numerical results (TDPFLEX and DEEPLINES).

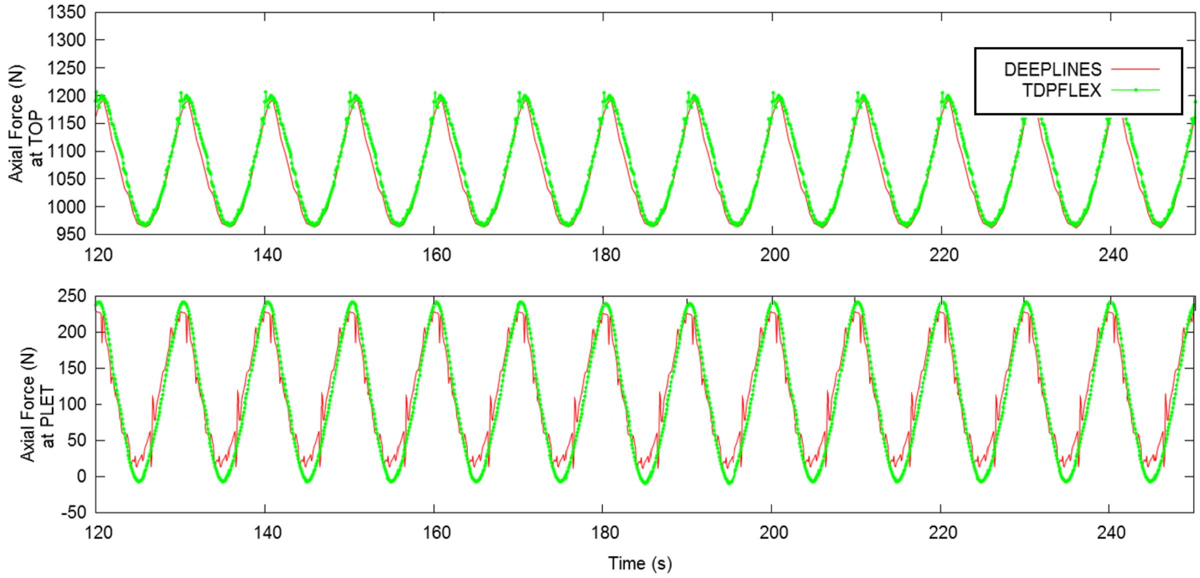

Fig. 5: Comparison between DEEPLINES and TDPFLEX axial forces at TOP and PLET

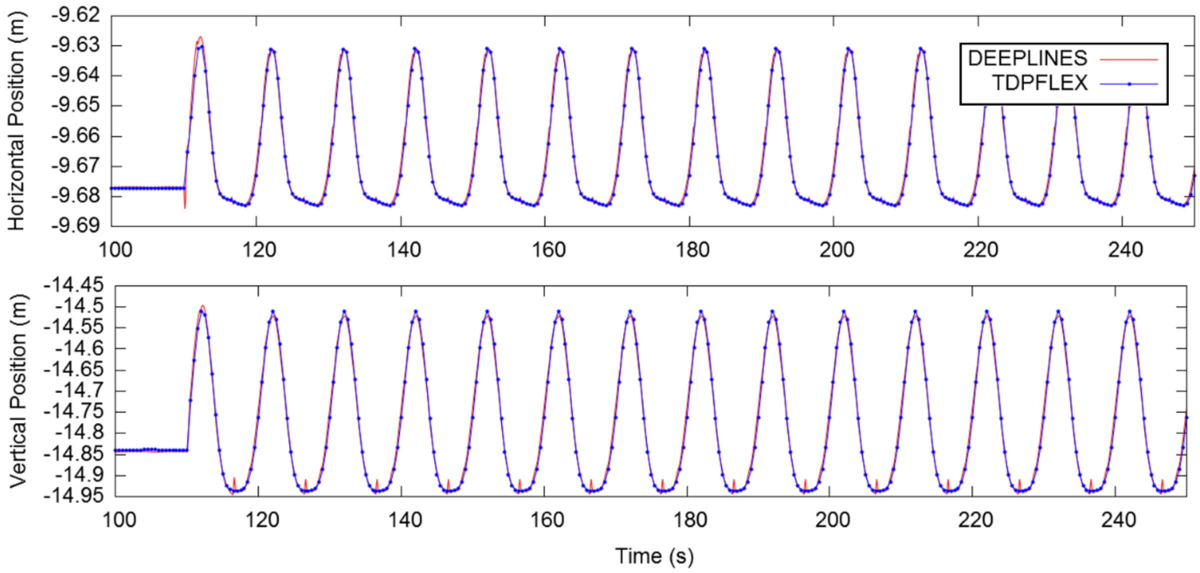

Fig. 6: Comparison between DEEPLINES and TDPFLEX horizontal and vertical positions near TDZ

4 CONCLUSION

This work presented the main aspects of an implementation of a bidimensional beam element with geometric nonlinearity.

The studied cases showed excellent agreement between a published example and the developed code. Additionally, the developed code was compared to the commercial software DEEPLINES for the verification of the algorithm, showing an excellent agreement too. For future work we intend to extend the implementation to a tridimentional formulation.

ACKNOWLEDGEMENTS

This work was partially supported by MCTI/FINEP, MCTI/CNPq and TechnipFMC Brasil.

REFERENCES

Bathe, K. J., 2006. *Finite element procedures*. Klaus-Jurgen Bathe.

Bhat, S., Dutta, A., Wu, J., & Sarkar, I., 2004. Pragmatic Solutions to Touch-Down Zone Fatigue Challenges in Steel Catenary Risers. *Offshore Technology Conference.* doi:10.4043/16627-MS

Chatjigeorgiou, I. K., 2008. A finite differences formulation for the linear and nonlinear dynamics of 2D catenary risers. *Ocean Engineering, 35*(7), 616-636.

Hughes, T. J., 2012. *The finite element method: linear static and dynamic finite element analysis*. Courier Dover Publications.

Kordkheili, S. A. H., Bahai, H., & Mirtaheri, M., 2011. An updated Lagrangian finite element formulation for large displacement dynamic analysis of three-dimensional flexible riser structures. *Ocean Engineering*, 38(5), 793-803.

O'Brien, P. J., & McNamara, J. F., 1989. Significant characteristics of three-dimensional flexible riser analysis. *Engineering structures, 11*(4), 223-233.

Paraski, N.V., 2012. *Análise Estática Não Linear de Pórticos Planos via Matlab.* Master's thesis, Universidade Federal Fluminense.

Przemieniecki, J. S., 1985. *Theory of matrix structural analysis*. Courier Dover Publications.

Souza, R.M., 2000. *Force-based Finite Element for Large Displacement Inelastic Analysis of Frames.* Doctoral dissertation, University of California, Berkeley.

Yazdchi, M., & Crisfield, M. A., 2002. Non-linear dynamic behaviour of flexible marine pipes and risers. *International journal for numerical methods in engineering*, *54*(9), 1265-1308.